Dependence of the dissipated energy of particles on the sizes and numbers of particles and balls in a planetary ball mill

Dependence of the dissipated energy of particles on the sizes and numbers of particles and balls in a planetary ball mill

Fumie Hirosawa and Tomohiro Iwasaki*

Department of Chemical Engineering, Osaka Prefecture University, Sakai, Osaka 599–8531, Japan

*Corresponding author:

    Tomohiro Iwasaki

    E-mail: iwasaki@chemeng.osakafu-u.ac.jp

    Postal address: 1–1 Gakuen-cho, Naka-ku, Sakai, Osaka 599–8531, Japan

    Tel: +81-72-254-9307, Fax: +81-72-254-9911

Abstract

The dissipated energy received by the particles during collisions in a high-energy ball-milling can vary due to the breakage and/or aggregation of the particles, that is, a change in the particle size. To investigate the energy variations, a numerical analysis of the behavior of particles and balls in a planetary ball mill was carried out under various conditions, considering different sizes and numbers of particles and balls using the discrete element method (DEM). The variable sizes and numbers of particles and balls affected the contact force, collision frequency, and types of particle collisions, resulting in variations in the dissipated energy distribution and specific dissipated power, even at a constant ball-to-particle filling mass ratio (BPR). The variation in specific dissipated power was expressed as a function of the sizes of the particles and balls and the BPR. According to the obtained empirical formula, the particle-to-ball size ratio strongly affects the specific dissipated power rather than the BPR. The results suggest that based on the energy variations with particle size and number, using balls of appropriate size and number can control the dissipated energy of particles, which may lead to the designing of energy-efficient milling processes.

Keywords

1. Introduction

High-energy ball mills, which include planetary ball mills, vibratory mills, and stirring mills (attritors), are widely used in various mechanical particle fabrication

processes, such as grinding, alloying, and mechanochemical reactions (Baláž et al., 2014, 2013; Dreizin and Schoenitz, 2017; Fuentes and Takacs, 2013; Leonardi et al., 2018; Mucsi, 2019; Suryanarayana, 2001) in many industries, ranging from coarse mineral ore to submicrometer-sized fine drug powder. The mechanical energy applied to the particles during milling in high-energy ball mills determines the properties and/or performance of the resultant particles. However, multiple factors such as operating conditions and physical properties of the particles affect the applied mechanical energy. The ball-to-particle filling mass ratio (BPR), defined as the amount of particles and balls placed in the mill pot, plays an important role in controlling the dissipated energy of the particles. Planetary ball mills are one of the most frequently used high-energy mills owing to their structural simplicity and good operability. Many researchers have used planetary ball mills with adjusted BPR to produce fine particles with controlled properties (Arnache et al., 2016; Chicardi et al., 2017; Chmielewski et al., 2010; Ghayour et al., 2016; Gotor et al., 2013; Hosseinzadeh et al., 2014; Li et al., 2020; Matijašić et al., 2008; Matsuoka et al., 2010; Patil and Anandhan, 2015; Shashanka and Chaira, 2015). Chmielewski et al. (2010) and Shashanka and Chaira (2015) demonstrated that for a mechanical alloying process conducted using a planetary ball mill, the average size of the milled particles was reduced by increasing the BPR. Even when the BPR is held constant, the sizes and numbers of particles and balls can significantly affect the properties of the resultant particles (Asadrokht and Zakeri, 2018; Bitterlich et al., 2014; Hien et al., 2012; Kuziora et al., 2014; Marin and Deleu, 2014; Vijay et al., 2013). Therefore, both BPR and sizes and numbers of particles and balls must be adjusted appropriately to control the properties of the resultant particles. When planetary ball mills are used, breakage and/or aggregation of the particles largely affect

the particle size and number, making precise control of the mechanical energy difficult.

Obtaining desired control of mechanical energy during milling is difficult to achieve solely by experimental approaches. Therefore, numerical simulation of the particle and ball behaviors using the discrete element method (DEM) (Cundall and Strack, 1979) has been used to estimate the mechanical energy. Agrawala et al. (1997), Mori et al. (2004), and Panjipour and Barani (2018) demonstrated that the DEM simulation can compute the ball behaviors accurately in tumbling mills by verifying the agreement of the calculated behaviors with the experimental one recorded using a high-speed camera. In case of planetary ball mills, where the motion of the balls is more aggressive than in tumbling mills, DEM can accurately simulate the behavior of the balls by comparison with actual behaviors (Rosenkranz et al., 2011). Moreover, DEM simulation has been used to estimate the mechanical energy related to particle breakage. Gudin et al. (2006) and Mori et al. (2004) reported the particle breakage rate and the estimated impact energy of grinding balls to be correlated irrespective of grinding conditions in a wet tumbling mill process. In planetary mills, Mio et al. (2004a, 2004b) demonstrated that the particle breakage rate was proportional to the impact energy of grinding balls. Therefore, DEM is a powerful tool for simulating solid particle behaviors and for obtaining the particle mechanical energy in planetary ball mills.

The simulation results (at least the ball motion in the vessel) must be verified through a comparison with the corresponding experimental data. Actually, some investigations confirmed that the calculated ball motion in a planetary mill was well coincided with the experimental observation using a high-speed camera as mentioned above. Based on the facts, Ashrafizadeh and Ashrafizaadeh (2012) produced noticeable results from the simulations; the total impact energy proportionably increased with an

increase of ball filling ratio in a planetary mill, although they showed no experimental data for directly confirming the validity of calculation results. Geissbuhler and Sawley (2013) also demonstrated in the absence of experimental data that an increase of particle filling mass led to a drastic reduction of the energy dissipation in a planetary mill. Based on the investigation by Geissbuhler and Sawley (2013), Mishra et al. (2015) proposed a multi-scale modeling approaches for a comminution. Moreover, the DEM simulation by Gusev et al. (2020) found that greatly larger impact energies were generated in a planetary mill with a square-shaped pot compared with that with a general cylindrical pot.

Using the mechanical energy obtained by the DEM simulation, various analyses of particle breakage can be performed. In particular, the dissipated energy can be used for the analysis of particle breakage rather than the impact energy. This is because the dissipated energy represents the energy loss during a collision, while the impact energy indicates the maximum kinetic energy associated with a collision. For example, the dissipated energy was used in a tumbling mill by Datta and Rajamani (2002) and Capece et al. (2014) to describe a numerical approach for evaluating the particle size and for formulating a particle breakage rate constant, respectively. Carvalho and Tavares (2013) and Tuzcu and Rajamani (2011), using the dissipated energy, investigated effects of operating conditions on particle breakage rates in a tumbling mill and in a SAG mill, respectively. Also in a stirred media mill, a multiscale modelling method to predict and optimize grinding processes was developed using the dissipated energy (Beinert et al., 2018). Cleary and Owen (2019) and Scott et al. (2021) investigated dissipated energy distributions to find milling conditions that particles can receive large dissipated energies in a SAG mill and in a jet mill, respectively. In

planetary mills, several researchers have analyzed the dependence of dissipated energy on the size and number of particles at a constant particle size and/or BPR (Ashrafizadeh and Ashrafizaadeh, 2012; Geissbuhler and Sawley, 2013; Hirosawa et al., in press). Therefore, to study the effects of the sizes and numbers of particles and balls on the dissipated energy with respect to the particle breakage stage during milling at various BPRs, the dissipated energy of particles must be analyzed under conditions of varying sizes and numbers of particles and balls.

This study systematically investigated the dependence of dissipated energy on the sizes and numbers of particles and balls at various values of BPR. We numerically analyzed the behavior of the particles and balls in a planetary ball mill under various milling conditions, considering different sizes and numbers of particles and balls attained using DEM simulations. As a model milling process for the simulation, the grinding process for silica glass particles (Capece et al., 2014) was employed in a planetary ball mill. To determine the parameters that affect the dissipated energy, we proposed an empirical formula that uses the sizes of particles and balls and the BPR as variables to describe dissipated energy.

2. Numerical analysis

2.1 Definition of dissipated energy

The dissipated energy (E) of particles can be defined as the energy dissipated by the damping force during a single contact. The damping force was determined by a dashpot in the DEM simulation during impact milling according to literature (Capece et al., 2014; Datta and Rajamani, 2002; Wang et al., 2012). The formula for dissipated energy is as follows:

$$E = \int_0^{t_c} (F_n \mathrm{d}\delta_n + F_t \mathrm{d}\delta_t), \qquad\qquad\qquad\qquad (1)$$

where F_n and F_t are the normal and tangential damping forces of a particle, respectively, δ_n and δ_t are its overlaps with the colliding particle, and t_c is the contact period. The total dissipated energy of particles was obtained by summing E for all particle collisions. The specific dissipated energy and the specific dissipated power were obtained by dividing the total energy with filling particle mass and by dividing the specific dissipated energy with milling time, respectively. To study the effects of the sizes and numbers of particles and balls on the specific dissipated power in detail, the dissipated power was analyzed separately by classifying it into three collision categories, namely particle-to-ball, particle-to-wall, and particle-to-particle collisions.

2.2 DEM simulation

To obtain the dissipated energy of particles, the motion of the particles and balls was simulated using DEM in a planetary ball mill under dry conditions (Hirosawa et al., 2019). We used an in-house DEM code for the simulation, that is based on the method proposed by Tsuji et al. (1992), and the Hertz-Mindlin contact model was used to estimate the contact force. The parameters used in the simulations are listed in Table 1. Generally, the contact parameters strongly affect the dissipated energy; hence they should be distinguished for collision types. However, within the range of conditions in this work, the variations in dissipated energy distribution with particle size were significantly larger than those with contact parameters as shown in Figs. S1a and S2a in the supplementary information. Moreover, variations in the dissipated energy distribution with respect to the ball size and BPR were almost the same as those even

when the contact parameters were changed widely (Figs. S1b, S1c, S2b and S2c). The results confirmed that we can investigate the variations in dissipated energy with sizes and numbers of particles and balls using representative contact parameters. Accordingly, as representative contact parameters, those used by Capece et al. (2014) were employed. Moreover, irrespective of the sizes and numbers of particles and balls, the densities of the particles and balls and the contact parameters were the same as those used by Capece et al. (2014). The revolution speed was kept constant at 600 rpm. To observe the variations in the dissipated energy of the particles with respect to sizes (D_p, D_b) and numbers (N_p, N_b) of particles and balls at various BPR values, the dissipated energies corresponding to the parameters given in Table 2 were calculated. In simulation run numbers 1–37 (Table 2), both D_p and N_p were changed individually at various BPR values and a constant D_b value in each simulation to investigate the variations in the dissipated energy with respect to the particle breakage stage. In contrast, in simulation run numbers 38–62, the energy variations with respect to D_b and N_b were investigated at a constant D_p. In this study, the total mass of the balls was kept constant (37.7 g) in all simulations, while the BPR was varied between 5 and 30, as shown in Table 2. Fig. 1 shows the change in specific dissipated power with the milling time for 100 revolutions of the mill pot under the conditions of run No. 1 as an example. The specific dissipated power varied periodically within a certain range after $t = 0.1$ s. Therefore, the total simulation time was 0.3 s, and the energy data was collected during the last 0.2 s.
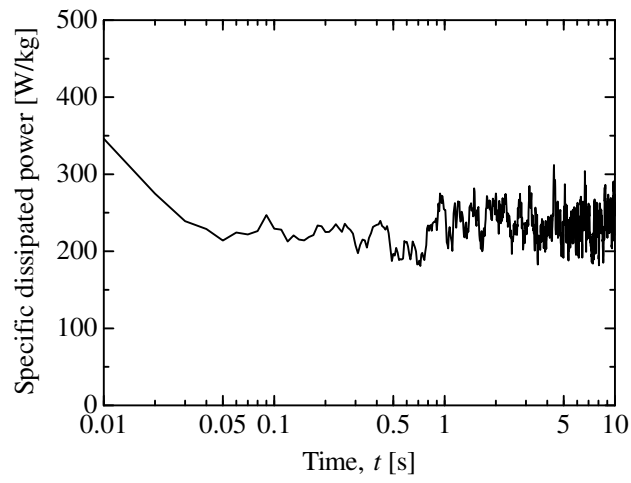
Fig. 1. Typical change in specific dissipated power of particles with milling time.

Table 1

Parameters used in simulations.

Number:	
Ball	8–52
Particle	18–6704
Ball/particle filling mass ratio (BPR)	5–30
Ball/particle filling volume ratio	2.7–16
Diameter:	
Ball	7.0–13.1 mm
Particle	0.67–4.0 mm
Density*:	
Ball, wall	4000 kg/m^3 (alumina)
Particle	2150 kg/m^3 (silica glass)
Pot volume	45 cm^3
Pot diameter	40 mm
Pot depth	35.8 mm
Revolution speed	600 rpm
Revolution radius	67 mm
Rotation-to-revolution speed ratio	–1
Time step	250 ns
Contact parameters:	
Poisson's ratio*	0.3
Young's modulus*	1×10^7 Pa
Coefficient of restitution*	0.75
Sliding friction coefficient*	0.75
Rolling friction coefficient*	0.02

*Capece et al. (2014)

Table 2

Sizes and numbers of particles and balls used in simulations.

Run No.	Particle diameter, D_p [mm]	Number of particles, N_p [–]	Ball diameter, D_b [mm]	Number of balls, N_b [–]	BPR [–]
1	4.0	18	10.0	18	30
2	2.7	59	10.0	18	30
3	2.0	140	10.0	18	30
4	1.6	273	10.0	18	30
5	1.3	476	10.0	18	30
6	1.0	1120	10.0	18	30
7	0.80	2188	10.0	18	30
8	0.67	3724	10.0	18	30
9	4.0	21	10.0	18	25
10	2.7	70	10.0	18	25
11	2.0	167	10.0	18	25
12	1.6	326	10.0	18	25
13	1.3	568	10.0	18	25
14	1.0	1336	10.0	18	25
15	0.80	2609	10.0	18	25
16	0.67	4442	10.0	18	25
17	4.0	26	10.0	18	20
18	2.7	88	10.0	18	20
19	2.0	209	10.0	18	20
20	1.6	408	10.0	18	20
21	1.3	711	10.0	18	20
22	1.0	1672	10.0	18	20
23	0.80	3266	10.0	18	20
24	0.67	5559	10.0	18	20
25	4.0	52	10.0	18	10
26	2.7	177	10.0	18	10
27	2.0	419	10.0	18	10
28	1.6	818	10.0	18	10
29	1.3	1425	10.0	18	10
30	1.0	3352	10.0	18	10
31	0.80	6547	10.0	18	10

Run No.	Particle diameter, D_p [mm]	Number of particles, N_p [–]	Ball diameter, D_b [mm]	Number of balls, N_b [–]	BPR [–]
32	4.0	105	10.0	18	5
33	2.7	354	10.0	18	5
34	2.0	838	10.0	18	5
35	1.6	1637	10.0	18	5
36	1.3	2829	10.0	18	5
37	1.0	6704	10.0	18	5
38	2.0	140	7.0	52	30
39	2.0	140	8.5	29	30
40 (3)*	2.0	140	10.0	18	30
41	2.0	140	11.5	12	30
42	2.0	140	13.1	8	30
43	2.0	167	7.0	52	25
44	2.0	167	8.5	29	25
45 (11)*	2.0	167	10.0	18	25
46	2.0	167	11.5	12	25
47	2.0	167	13.1	8	25
48	2.0	209	7.0	52	20
49	2.0	209	8.5	29	20
50 (19)*	2.0	209	10.0	18	20
51	2.0	209	11.5	12	20
52	2.0	209	13.1	8	20
53	2.0	419	7.0	52	10
54	2.0	419	8.5	29	10
55 (27)*	2.0	419	10.0	18	10
56	2.0	419	11.5	12	10
57	2.0	419	13.1	8	10
58	2.0	838	7.0	52	5
59	2.0	838	8.5	29	5
60 (34)*	2.0	838	10.0	18	5
61	2.0	838	11.5	12	5
62	2.0	838	13.1	8	5

*Runs No. 40, 45, 50, 55, and 60 are the same as runs No. 3, 11, 19, 27, and 34, respectively.

3. Results and discussion

3.1 Effect of size and number of particles on dissipated energy

The results obtained from the simulation in this work are shown below. Fig. 2 illustrates snapshots of the states of the particles and balls in the mill pot at different values of D_p and BPR. Large and small D_p mimic the early and final stages of particle breakage, respectively. A decrease in the D_p at a constant D_b represents a progress of the particle breakage stage by milling. Under all conditions, the balls were packed near the wall of the mill pot, even when the particle size was changed. The action is justified by the strong centrifugal acceleration induced by the planetary motion. Notably, at high BPRs, the small particles tended to gather near the wall because of their ability to pass through voids between the balls. In contrast, at low BPRs, the void spaces near the wall were almost entirely occupied by the particles, and a large number of particles were located not only near the wall of the mill pot but also around its center. The similar particle behaviors were observed in a tumbling mill (Cleary and Morrison, 2011). The particles were packed at the shoulder region in the tumbling mill at high BPRs. In contrast, at low BPRs, the particles were located not only at the shoulder region but also at the toe region. These results show that, at high BPRs, the particles tend to gather in certain regions in the mill pot in planetary mills as well as tumbling mills. Therefore, in planetary mills, particles may receive large amounts of the dissipated energy via particle-to-ball and particle-to-wall collisions at high BPRs and via particle-to-ball and particle-to-particle collisions at low BPRs.
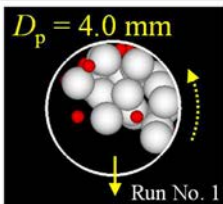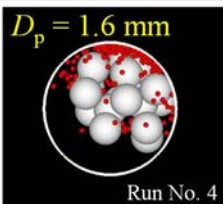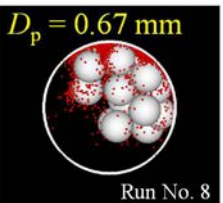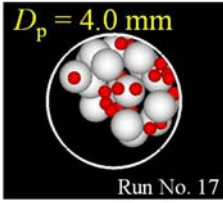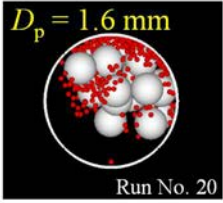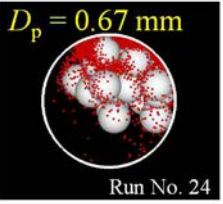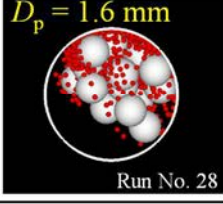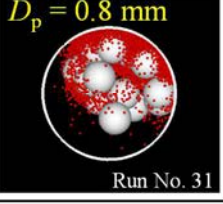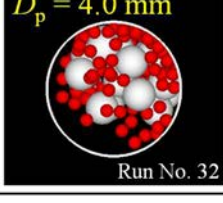
Fig. 2. Snapshots of behaviors of particles and balls mimicking various stages of particle breakage at different values of BPR (D_b = 10 mm).

To analyze the dissipated energy, normal damping force was used. This is because the dissipated energy generated by the normal damping force was significantly larger than that by the tangential force in this system. For example, in run No. 1, the values of specific dissipated power in the normal and tangential directions were 0.21 kW/kg and 0.016 kW/kg, respectively. The observation confirmed the limited impact of tangential damping force on the dissipated energy. Fig. 3 shows the variations in

dissipated energy distribution of all collisions (i.e., total of particle-to-ball, particle-to-particle, and particle-to-wall collisions) with D_p at different BPRs. Irrespective of the BPRs, the significant decrease in the dissipated energy with decreasing D_p was observed due to reductions in a single particle mass.
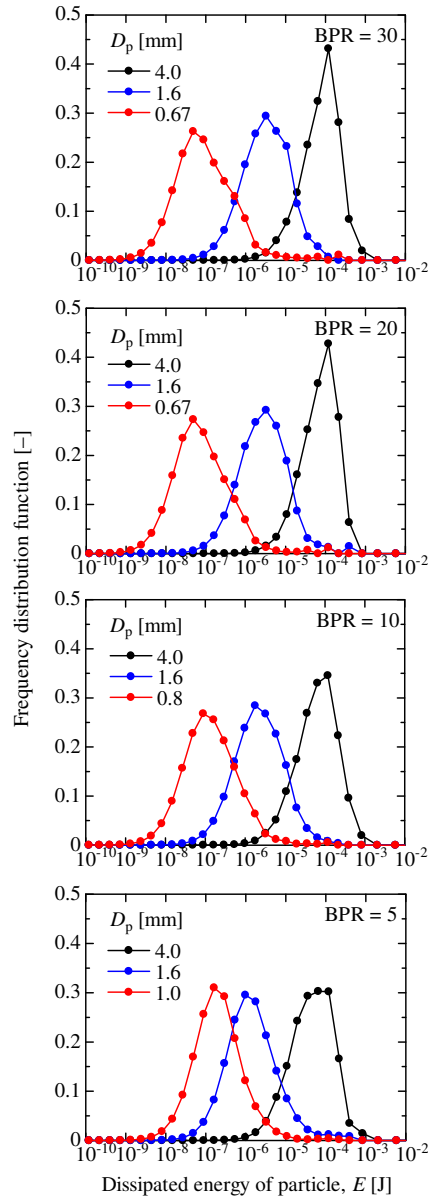

Fig. 3. Effect of D_p on dissipated energy distribution of all collisions at different values of BPR ($D_b = 10$ mm).

To investigate the effects of D_p, D_b, and BPR on dissipated energy, which successively contributes to particle breakage, we estimated the specific dissipated power (E_s) for particles that exceeded the threshold energy (E_{th}) for particle breakage. According to Capece et al. (2014), the particle fracture begins when E surpasses E_{th}. The E_{th} for a single particle collision is defined by Eq. (2) (Capece et al., 2014):

$$E_{th} = E_{min}m_p/D_p, \tag{2}$$

where m_p refers to the mass of a single particle and E_{min} is a size-independent material property referred to as the E_{th} of breakage, as proposed by Capece et al. (2014); for example, $E_{min} = 2.6 \times 10^{-3}$ J·m/kg for silica glass particles. In this study, when D_p was changed from 4.0 to 0.67 mm, E_{th} decreased from 4.6×10^{-5} to 1.3×10^{-6} J. Fig. 4 demonstrates the variations in E_s with D_p for the three different collision types, at BPR values of 30 and 5 (run numbers 1–8, 32–37). The values of E_s for particle-to-ball and particle-to-wall collisions were greater than that of particle-to-particle collisions at BPR = 30. However, at BPR = 5, E_s for particle-to-particle collisions was larger than that of particle-to-wall collisions. This is because the void spaces near the wall were almost entirely occupied by the particles (Fig. 2) and the number of particle-to-particle collisions was significantly higher (i.e., approximately four times higher at large D_p) than that of particle-to-wall collisions. Also in a tumbling mill, the energy generated at particle-to-ball collisions was greatly larger than that at particle-to-particle collisions (Wang et al., 2012). Moreover, the difference between the energy generated at particle-to-ball collisions and that at particle-to-particle collisions (Wang et al., 2012) was larger than the difference in the planetary mill obtained from our simulation. The results suggest that the particles in the planetary mill were more densely packed by the

16

balls compared with the cases in the tumbling mill, resulting in generation of relatively large dissipated energies even at particle-to-particle collisions in the planetary mill. In general, quite large dissipated energy can generate in ball mills when particles are directly captured with balls and/or wall (i.e., ball-particle-ball and ball-particle-wall collisions) (Rodriguez et al., 2018), and the energy can contribute to the particle breakage effectively. In this work, the energy contributed to particle breakage was expressed by E_s which reflected the energy exceeding the threshold E_{th} of particle breakage. Therefore, the variation in dissipated energy spent for the particle breakage with sizes and numbers of particles and balls can be analyzed based on the E_s variations without considering the energy for individual collisions. However, it is needed for analyzing the differences in the dissipated energy by collision types in more detail. We will deal with the collisions individually and report the results elsewhere in future. As shown in Fig. 4, at BPR values of 30 and 5, E_s for all the three collision types notably decreased with decreasing D_p because the dissipated energy distributions shifted toward lower energy ranges (Fig. 2). Fig. 5 illustrates the variation in E_s for all collisions (i.e., total of particle-to-ball, particle-to-wall, and particle-to-particle collisions) with respect to D_p and BPR; the calculated values of E_s are located at the intersections of the white grid, and the regions between the gridlines are filled using interpolation. The areas within the grid that are filled in black correspond to parameters that are not within the ranges examined in this study. Even at a constant BPR, the E_s for all collisions decreased significantly with decreasing D_p. However, E_s gradually decreased with the reduction of BPR. The results suggest that E_s is strongly affected by the D_p rather than the BPR.
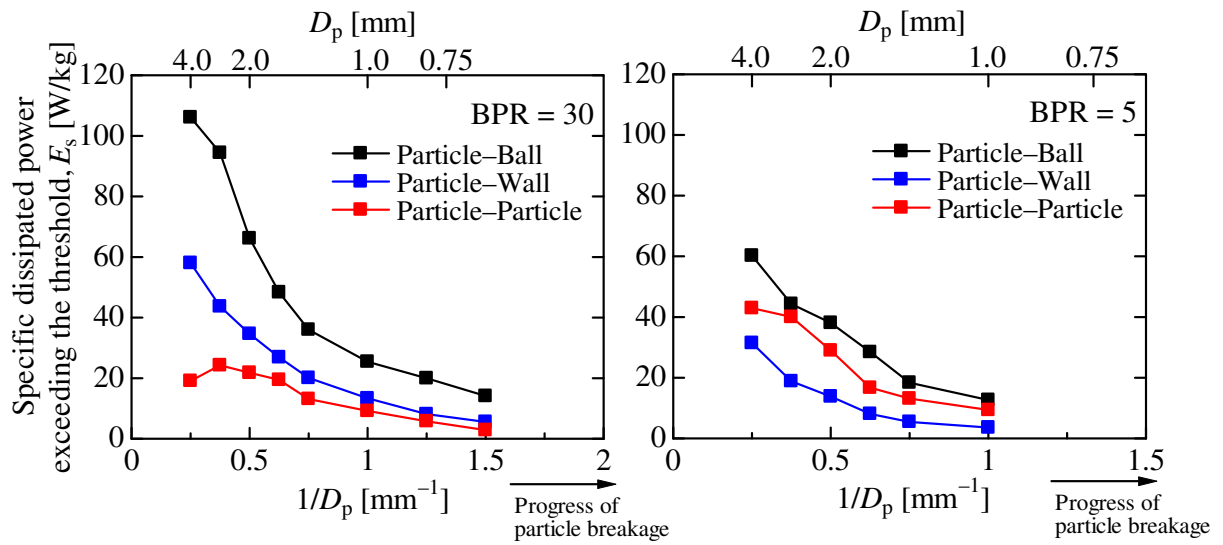
17

Fig. 4. Effect of D_p on E_s for particle-to-ball, particle-to-wall, and particle-to-particle collisions at BPR = 30 and 5 (D_b = 10 mm).
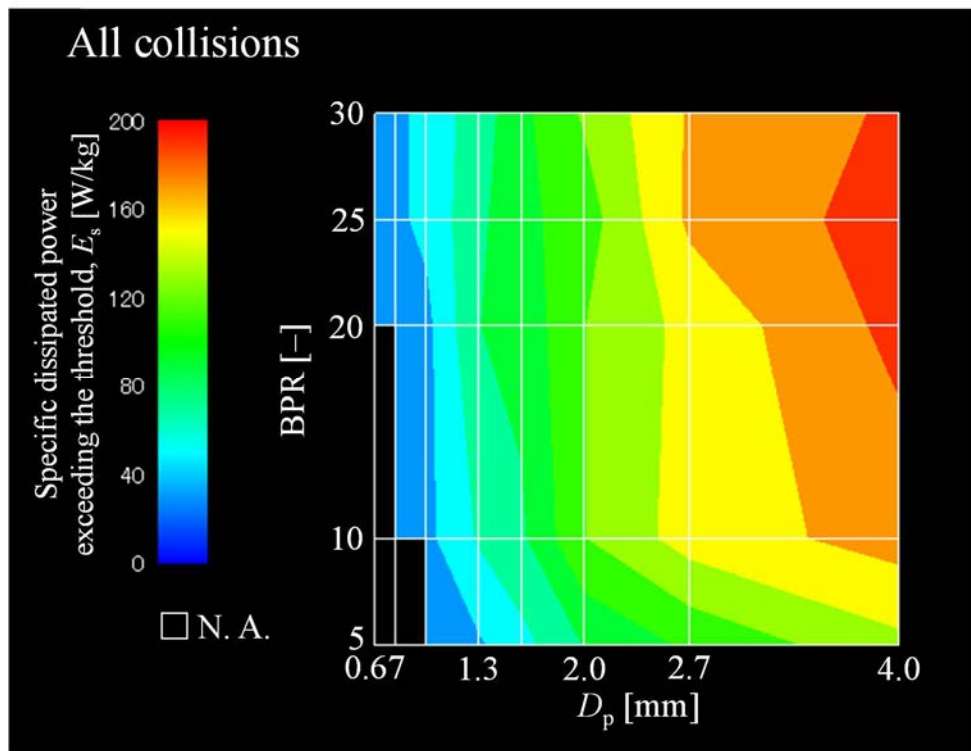

Fig. 5. Variations in E_s for all collisions with respect to D_p and BPR (D_b = 10 mm).

3.2 Effect of size and number of balls on dissipated energy

Fig. 6 illustrates the snapshots of particles and balls in the mill pot at a constant D_p and with different values of D_b and BPRs. Similar to the cases shown in Fig. 2, the balls were packed densely near the wall of the mill pot. The use of small sized balls reduced the void spaces among the densely packed balls, suggesting that a large number of particles can be trapped between the packed balls. These particles can collide with the balls, generating a relatively large amount of dissipated energy.
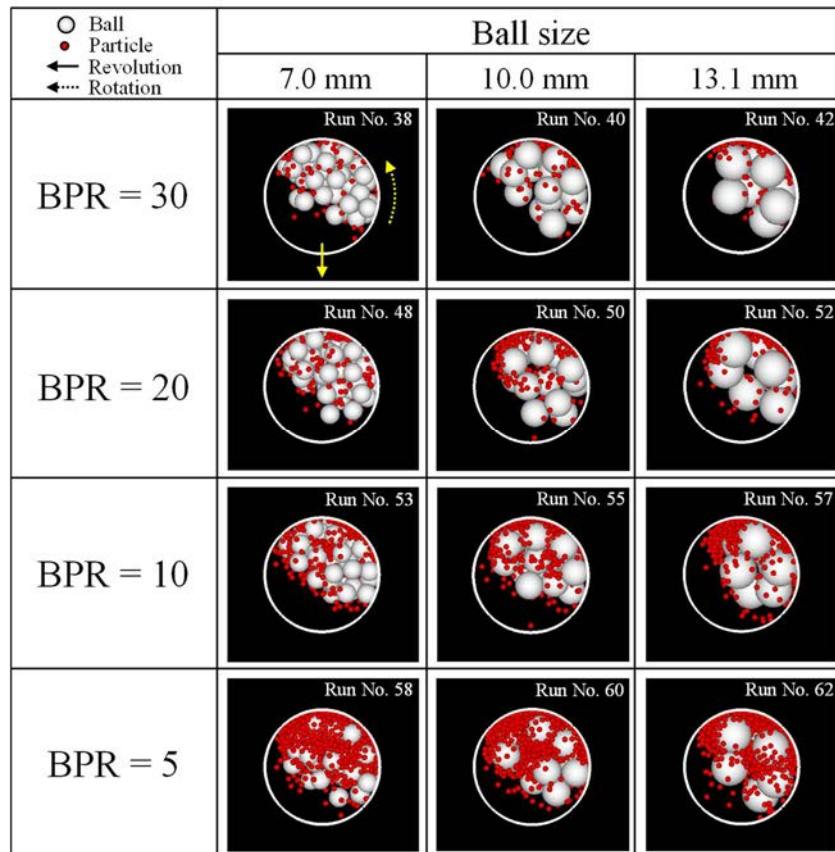

Fig. 6. Changes in behaviors of particles and balls with ball size at different values of BPR ($D_p = 2.0$ mm).

Fig. 7 shows the variations in the dissipated energy distribution with respect to D_b at a constant D_p and different values of BPR. Except at BPR = 5, the distribution curves slightly shifted to the higher energy ranges as D_b decreased. This primarily owes to the large amounts of dissipated energy generated by the particle-to-ball collision of the particles trapped between the packed balls, as shown in Fig. 6. Also, in a tumbling mill, small balls can easily capture the particles; hence the similar energy variation with D_b was observed (Rodriguez et al., 2018) to that in the planetary mill shown in Fig. 7. As shown in Fig. 7, the distribution curves slightly shifted toward the lower energy ranges with decreasing BPR because the number of particle-to-particle collisions greatly increased. Actually, the number of particle-to-particle collisions at BPR = 5 was approximately 20 times larger than that at BPR = 30 for D_b = 10 mm.
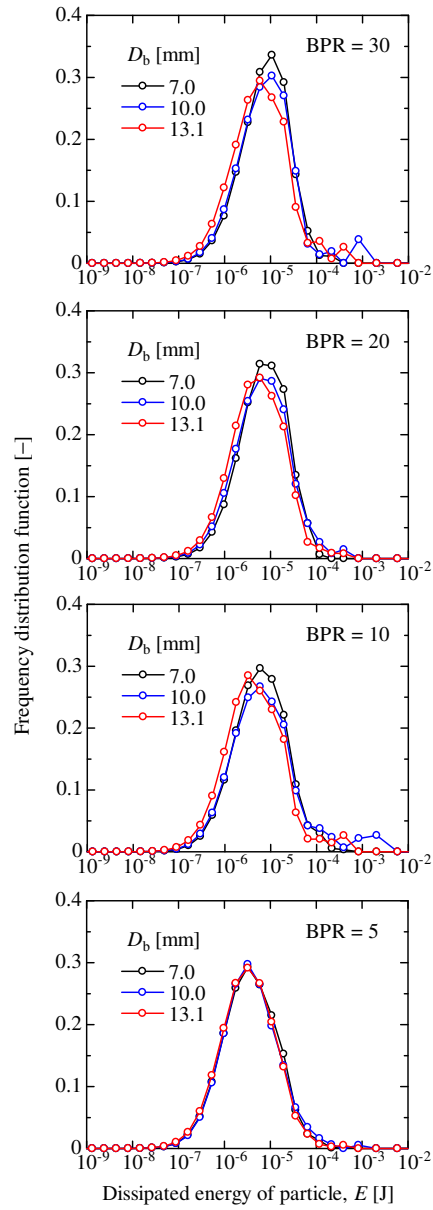
Fig. 7. Effect of D_b on dissipated energy distribution of all collisions at different values of BPR (D_p = 2.0 mm).

Fig. 8 demonstrates the variations in E_s with D_b for the three different collision types, at BPR values of 30 and 5. At the high BPR, E_s for particle-to-ball collisions was greatly large when small balls were used due to a large number of particles trapped

21

between the packed balls as shown in Fig. 6. In contrast, when D_b was large, E_s for particle-to-ball collisions and particle-to-particle collisions were gradually decreased and increased, respectively, because a few particles could be trapped between the packed balls, regardless of the BPR. Fig. 9 shows the variations in E_s for all collisions with respect to D_b and BPR. The E_s for all collisions increased with decreasing D_b and increasing BPR. This could be justified by the increase in E_s for particle-to-ball collisions (Fig. 8). The variation in E_s with respect to D_b was smaller than that with D_p, as shown in Fig. 5. The results suggest that the particle-to-ball size ratio can affect E_s more strongly.
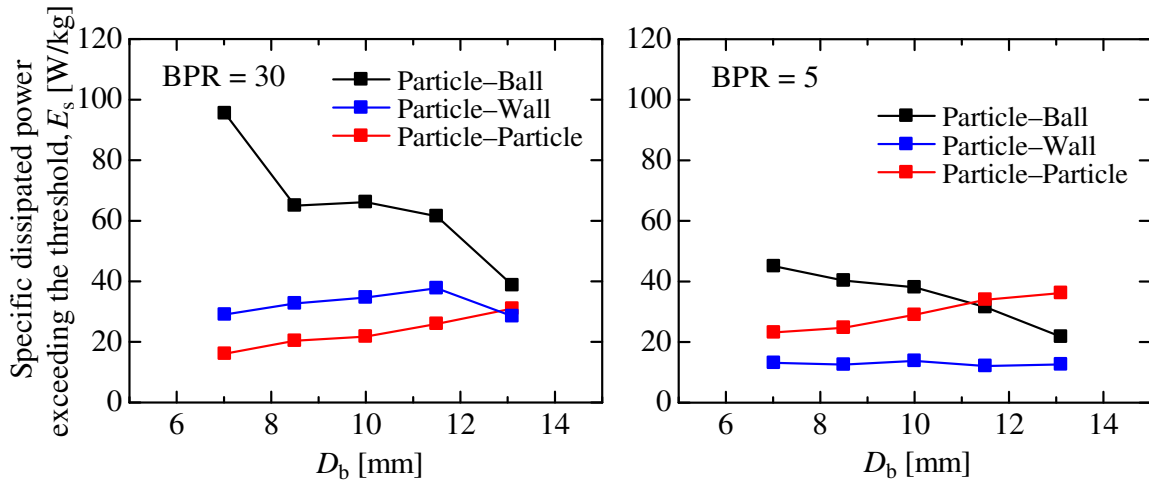

Fig. 8. Effect of D_b on E_s for particle-to-ball, particle-to-wall, and particle-to-particle collisions at BPR = 30 and 5 (D_p = 2.0 mm).
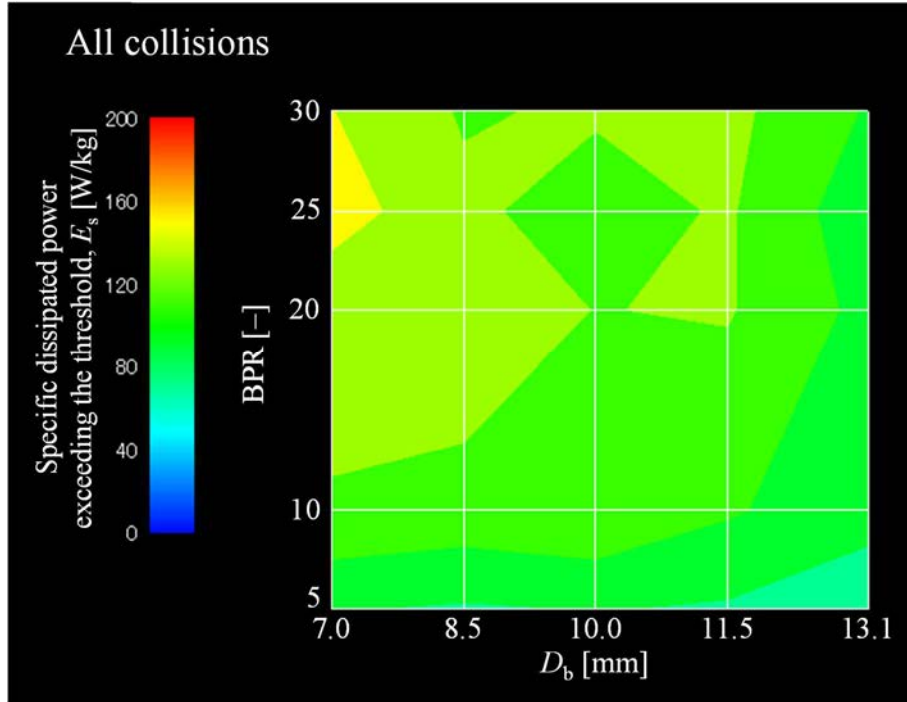
Fig. 9. Variations in E_s for all collisions with respect to D_b and BPR ($D_p = 2.0$ mm).

3.3 Determination of parameters governing dissipated energy of particles

To appropriately adjust the dissipated energy applied to the particles during milling, it is essential to determine parameters that control the dissipated energy. By investigating the parameters influencing dissipated energy, Beinert et al. (2015) formulated a function expressing the relationship between grinding power and several operating conditions such as the size, density, and number of balls and the rotational speed of the mill pot in a planetary ball mill. In this study, considering that E_s is strongly affected not only by D_b, N_b, and m_b (mass of the balls), but also by D_p, N_p, and m_p, we assumed that the correlation between E_s and these parameters related to the particles and balls could be expressed numerically by Eq. (3):

$$E_s = C_1 \cdot (D_p / D_b)^{C_2} \cdot (\text{BPR})^{C_3},$$ (3)

where C_1, C_2, and C_3 are the coefficients. The effects of N_b, m_b, N_p, and m_p on the E_s are captured by the BPR, i.e., BPR = $N_b m_b / N_p m_p$. By applying Eq. (3) to E_s values obtained from the simulations, using different values of the parameters to determine C_1, C_2, and C_3 with the least-squares method, Eq. (4) was obtained.

$$E_s = 2.4 \times 10^2 \cdot (D_p / D_b)^{0.87} \cdot (\text{BPR})^{0.20}.$$ (4)

Fig. 10 shows a comparison of E_s values estimated using Eq. (4) with those obtained from the simulations. The observation demonstrates that the relationship between E_s and the parameters representing the sizes, numbers, and masses of particles and balls can be captured appropriately using Eq. (4). Furthermore, Eq. (4) indicates that the degree of dependence of E_s on D_p/D_b was higher than that on BPR.

According to Kwan et al. (2005), the grinding rate constant is proportional to the milling power, which decreases with reduced particle size. This suggests that the energy spent for particle breakage should be kept at high values to ensure efficient progress of the particle breakage. As expressed in Eq. (4), the D_p/D_b strongly affects E_s, suggesting that the balls should be replaced with those of a different size and/or the mixture of balls of different sizes should be used in accordance with the variation in particle size distribution caused by the particle breakage. This ensures that particles receive suitable dissipated energy. Based on the results obtained, we attempted to control the dissipated energy by using a D_b suitable for the D_p. For a batch grinding process in accordance with the stages of particle breakage, that is, the decrease of D_p from 2.7 to 1.3 mm at a constant particle filling mass, the D_b and N_b were changed from 10.0 mm and 6 (Run

24

No. 63) to 5.0 mm and 210 (Run No. 66), respectively, as shown in Table 3. Fig. 11 depicts the variations in E_s. The values of E_s calculated in run numbers 63–66 was better controlled compared with E_s obtained under the conditions where D_b and N_b were maintained at $D_b = 10.0$ mm and $N_b = 18$. The results suggest that using an appropriate size and number of balls in accordance with the stages of particle breakage is effective for precisely controlling the dissipated energy of particles.
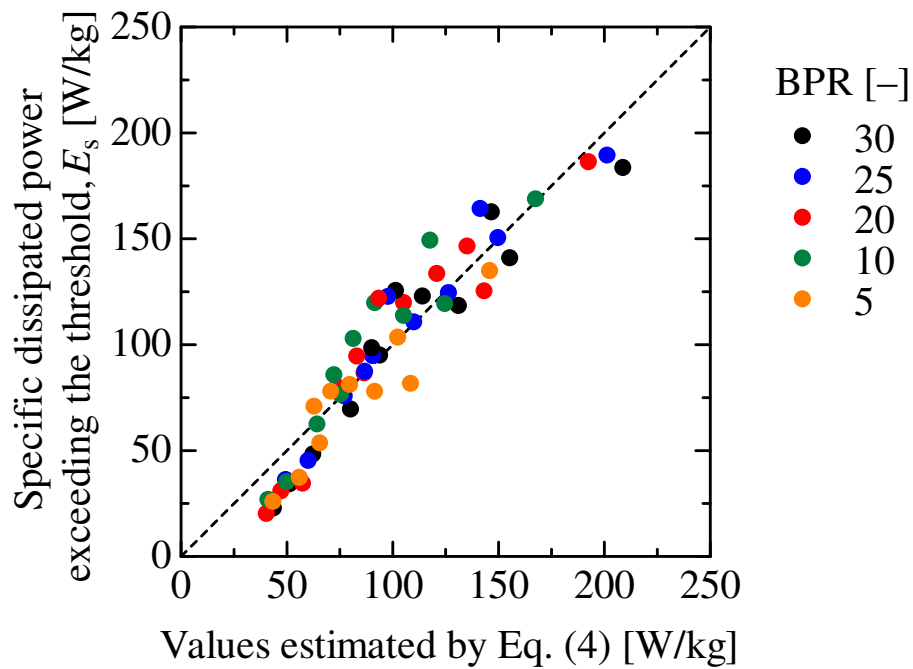

Fig. 10. Application of Eq. (4) for estimating E_s.

Table 3

Example of variation in milling conditions with decreasing particle size to maintain energy.

Run No.	D_p [mm]	N_p [–]	D_b [mm]	N_b [–]
63	2.7	88	10.0	6
64	2.0	209	8.0	15
65	1.6	408	6.0	107
66	1.3	711	5.0	210

*Particle filling mass was kept at 1.9 g in each batch.
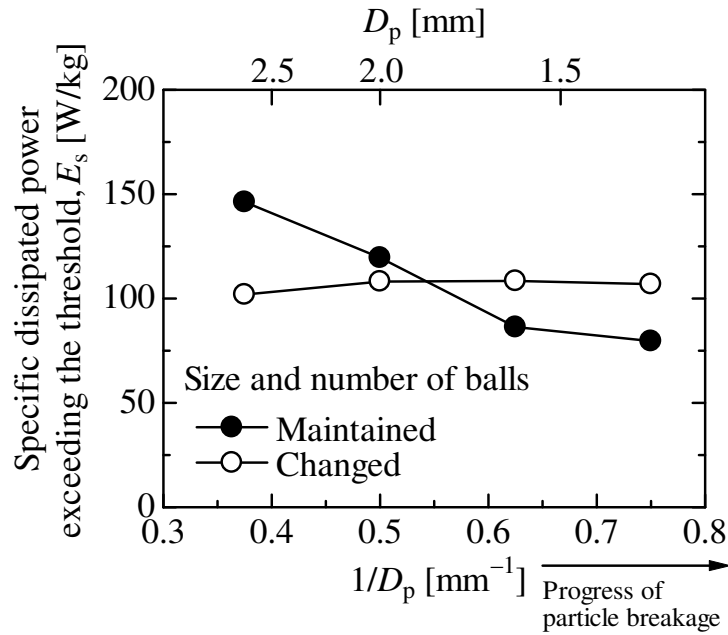

Fig. 11. Effect of changing D_b and N_b on variation in E_s with particle breakage stage.

4. Conclusions

The dissipated energy of particles that exceeds the threshold corresponding to the particle breakage in a planetary ball mill was analyzed based on DEM simulations of the behavior of the particles and balls. Even when the BPR was maintained at a constant

value, the specific dissipated energy exceeding the threshold depended strongly on the sizes and numbers of particles and balls, due to the variations in the dissipated energy distribution. The unique results of the work were as follows:

(i) The variation in the specific dissipated power exceeding the threshold was expressed as a function that included the size ratio of particle to ball and the BPR value as variables.

(ii) The effect of the sizes of particles and balls on the specific dissipated power exceeding the threshold was significant, compared with that of BPR.

(iii) The specific dissipated power exceeding the threshold could be controlled by changing the size and number of balls with respect to the particle size even when the particle size decreased.

The results suggest that the size and number of balls should be determined appropriately, in accordance with the particle breakage stage to effectively control the particle dissipated energy.

Appendix A. Supplementary data

The following are supplementary data to this article:

Supplementary_Data.pdf

Supplementary information:
Dependence of the dissipated energy of particles on the sizes and numbers of particles and balls in a planetary ball mill

Fumie Hirosawa and Tomohiro Iwasaki*

Department of Chemical Engineering, Osaka Prefecture University, Sakai, Osaka 599–8531, Japan
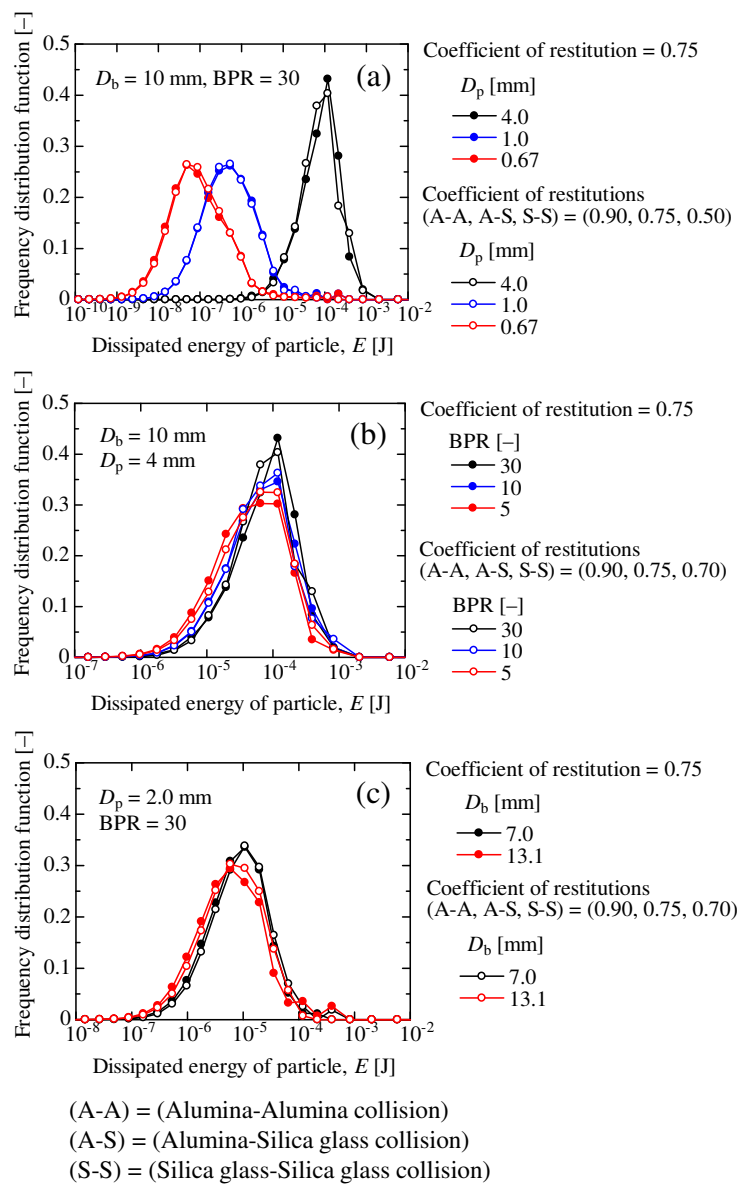
Fig. S1. Variation in dissipated energy distributions with coefficient of restitutions.
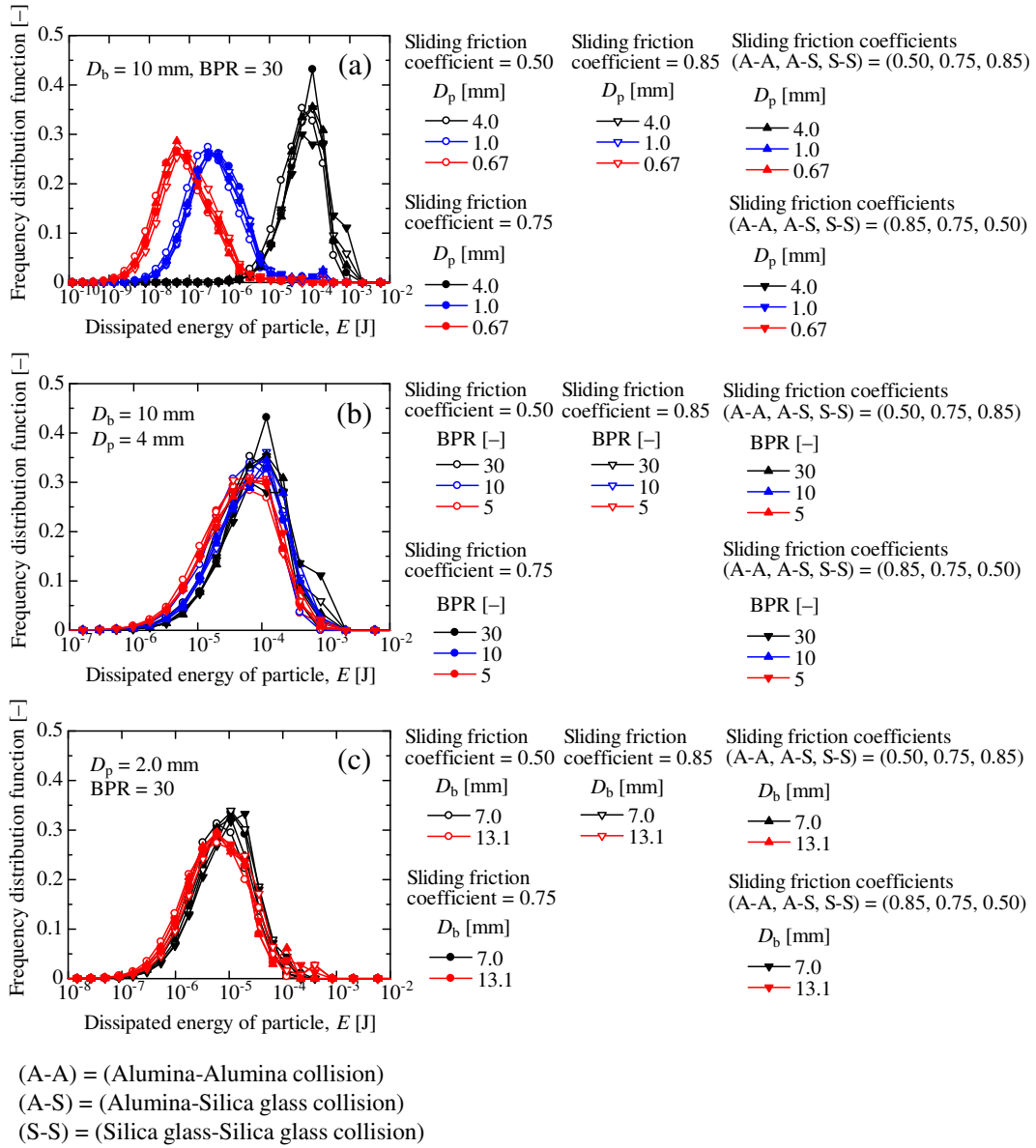
(A-A) = (Alumina-Alumina collision)
(A-S) = (Alumina-Silica glass collision)
(S-S) = (Silica glass-Silica glass collision)

Fig. S2. Variation in dissipated energy distributions with sliding friction coefficients.

References

Agrawala, S., Rajamani, R.K., Songfack, P., Mishra, B.K., 1997. Mechanics of media motion in tumbling mills with 3d discrete element method. Miner. Eng. 10, 215–227. https://doi.org/10.1016/S0892-6875(96)00147-1

Arnache, O.L., Pino, J., Sánchez, L.C., 2016. Determination of milling parameters useful on the formation of $CoSb_3$ thermoelectric powders by low-energy mechanical alloying. J. Mater. Sci.: Mater. Electron. 27, 4120–4130. http://dx.doi.org/10.1007/s10854-016-4271-5

Asadrokht, M., Zakeri, A., 2018. Effect of concurrent ball milling on cementation reactions: the case of Cu-Al system. Miner. Eng. 125, 15–25. https://doi.org/10.1016/j.mineng.2018.05.024

Ashrafizadeh, H., Ashrafizaadeh, M., 2012. Influence of processing parameters on grinding mechanism in planetary mill by employing discrete element method. Adv. Powder Technol. 23, 708–716. http://dx.doi.org/10.1016/j.apt.2011.09.002

Baláž, P., Achimovičová, M., Baláž, M., Billik, P., Cherkezova-Zheleva, Z., Criado, J.M., Delogu, F., Dutková, E., Gaffet, E., Gotor, F.J., Kumar, R., Mitov, I., Rojac, T., Senna, M., Streletskii, A., Wieczorek-Ciurowa, K., 2013. Hallmarks of mechanochemistry: from nanoparticles to technology. Chem. Soc. Rev. 42, 7571–7637. https://doi.org/10.1039/C3CS35468G

Baláž, P., Baláž, M., Bujňáková, Z., 2014. Mechanochemistry in technology: from minerals to nanomaterials and drugs. Chem. Eng. Technol. 37, 747–756. https://onlinelibrary.wiley.com/doi/pdf/10.1002/ceat.201300669

Beinert, S., Fragnière, G., Schilde, C., Kwade, A., 2015. Analysis and modelling of bead contacts in wet-operating stirred media and planetary ball mills with CFD–DEM

simulations. Chem. Eng. Sci. 134, 648–662.

http://dx.doi.org/10.1016/j.ces.2015.05.063

Beinert, S., Fragnière, G., Schilde, C., Kwade, A., 2018. Multiscale simulation of fine

grinding and dispersing processes: stressing probability, stressing energy and

resultant breakage rate. Adv. Powder Technol. 29, 573–583.

https://doi.org/10.1016/j.apt.2017.11.034

Bitterlich, A., Laabs, C., Busmann, E., Grandeury, A., Juhnke, M., Bunjes, H., Kwade,

A., 2014. Challenges in nanogrinding of active pharmaceutical ingredients.

Chem. Eng. Technol. 37, 840–846.

https://onlinelibrary.wiley.com/doi/pdf/10.1002/ceat.201300697

Capece, M., Bilgili, E., Davé, R., 2014. Insight into first-order breakage kinetics using a

particle-scale breakage rate constant. Chem. Eng. Sci. 117, 318–330.

http://dx.doi.org/10.1016/j.ces.2014.06.019

Carvalho, R.M., Tavares, L.M., 2013. Predicting the effect of operating and design

variables on breakage rates using the mechanistic ball mill model. Miner. Eng.

43–44, 91–101. https://doi.org/10.1016/j.mineng.2012.09.008

Chicardi, E., Gotor, F.J., Alcalá, M.D., Córdoba, J.M., 2017. Influence of milling

parameters on the solid-gas synthesis of TiC_xN_{1-x} by mechanically induced

self-sustaining reaction. Powder Technol. 319, 12–18.

http://dx.doi.org/10.1016/j.powtec.2017.06.035

Chmielewski, M., Kaliński, D., Pietrzak, K., Włosiński, W., 2010. Relationship between

mixing conditions and properties of sintered 20AlN/80Cu composite materials.

Arch. Metall. Mater. 55, 579–585.

http://imim.pl/files/archiwum/Vol2_2010/22.pdf

Cleary, P.W., Morrison, R.D., 2011. Understanding fine ore breakage in a laboratory
    scale ball mill using DEM. Miner. Eng. 24, 352–366.
    https://doi.org/10.1016/j.mineng.2010.12.013

Cleary, P.W., Owen, P., 2019. Effect of operating condition changes on the collisional
    environment in a SAG mill. Miner. Eng. 132, 297–315.
    https://doi.org/10.1016/j.mineng.2018.06.027

Cundall, P.A., Strack, O.D.L., 1979. A discrete numerical model for granular assemblies.
    Géotechnique 29, 47–65.

Datta, A., Rajamani, R.K., 2002. A direct approach of modeling batch grinding in ball
    mills using population balance principles and impact energy distribution. Int. J.
    Miner. Process. 64, 181–200. https://doi.org/10.1016/S0301-7516(01)00044-8

Dreizin, E.L., Schoenitz, M., 2017. Mechanochemically prepared reactive and energetic
    materials: a review. J. Mater. Sci. 52, 11789–11809.
    https://doi.org/10.1007/s10853-017-0912-1

Fuentes, A.F., Takacs, L., 2013. Preparation of multicomponent oxides by
    mechanochemical methods. J. Mater. Sci. 48, 598–611.
    https://doi.org/10.1007/s10853-012-6909-x

Geissbuhler, D., Sawley, M.L., 2013. Particle motion and energy dissipation spectra in a
    planetary ball mill. Proc. III International Conference on Particle-based Methods
    – Fundamentals and Applications (PARTICLES 2013), Stuttgart, Germany, pp.
    236–246.

Ghayour, H., Abdellahi, M., Bahmanpour, M., 2016. Optimization of the high energy
    ball-milling: modeling and parametric study. Powder Technol. 291, 7–13.
    http://dx.doi.org/10.1016/j.powtec.2015.12.004

Gotor, F.J., Achimovicova, M., Real, C., Balaz, P., 2013. Influence of the milling

parameters on the mechanical work intensity in planetary mills. Powder Technol.

233, 1–7. http://dx.doi.org/10.1016/j.powtec.2012.08.031

Gudin, D., Turczyn, R., Mio, H., Kano, J., Saito, F., 2006. Simulation of the movement

of beads by the DEM with respect to the wet grinding process. AIChE J. 52,

3421–3426. https://doi.org/10.1002/aic.10956

Gusev, V.G., Sobolkov, A.V., Aborkin, A.V., 2020. Increasing of energy-power

indicators of mechanical processing in a planetary mill by the use of a working

chamber with a square shape of the internal cavity. Solid State Phenom. 299,

447–451. https://doi.org/10.4028/www.scientific.net/SSP.299.447

Hien, T.T.T., Shirai, T., Fuji, M., 2012. Mechanical modification of silica powders. J.

Ceram. Soc. Jpn. 120, 429–435. https://doi.org/10.2109/jcersj2.120.429

Hirosawa, F., Iwasaki, T., Iwata, M., 2019. Kinetic analysis of mechanochemical

reaction between zinc oxide and gamma ferric oxide based on the impact energy

and collision frequency of particles. Powder Technol. 352, 360–368.

https://doi.org/10.1016/j.powtec.2019.04.050

Hirosawa, F., Iwasaki, T., Iwata, M., Particle impact energy variation with the size and

number of particles in a planetary ball mill. MATEC Web of Conf.

(APCChE2019), in press.

Hosseinzadeh, L., Baedi, J., Zak, A.K., 2014. X-ray peak broadening analysis of

$Fe_{50}Ni_{50}$ nanocrystalline alloys prepared under different milling times and BPR

using size strain plot (SSP) method. Bull. Mater. Sci. 37, 1147–1152.

https://www.ias.ac.in/article/fulltext/boms/037/05/1147-1152

Kuziora, P., Wyszyńska, M., Polanski, M., Bystrzycki, J., 2014. Why the ball to powder

ratio (BPR) is insufficient for describing the mechanical ball milling process. Int. J. Hydrogen Energ. 39, 9883–9887. http://dx.doi.org/10.1016/j.ijhydene.2014.03.009

Kwan, C.C., Mio, H., Chen, Y.Q., Ding, Y.L., Saito, F., Papadopoulos, D.G., Bentham, A.C., Ghadiri, M., 2005. Analysis of the milling rate of pharmaceutical powders using the Distinct Element Method (DEM). Chem. Eng. Sci. 60, 1441–1448. https://doi.org/10.1016/j.ces.2004.10.002

Leonardi, M., Villacampa, M., Menéndez, J.C., 2018. Multicomponent mechanochemical synthesis, Chem. Sci. 9, 2042–2064. https://doi.org/10.1039/c7sc05370c

Li, H., Tan, C., Wu, L., Zhang, Z., Jin, Y., Yang, Z., 2020. Mechanochemical immobilization of lead smelting slag using quartz sand. Miner. Eng. 151, 106303. https://doi.org/10.1016/j.mineng.2020.106303

Marin, B.J., Deleu, H., 2014. Grinding of vegetal fibers to micrometer size. Chem. Eng. Technol. 37, 888–890. https://onlinelibrary.wiley.com/doi/pdf/10.1002/ceat.201300640

Matijašić, G., Žižek, K., Glasnović, A., 2008. Suspension rheology during wet comminution in planetary ball mill. Chem. Eng. Res. Des. 86, 384–389. https://doi.org/10.1016/j.cherd.2007.11.013

Matsuoka, M., Hirata, J., Yoshizawa, S., 2010. Kinetics of solid-state polymorphic transition of glycine in mechano-chemical processing. Chem. Eng. Res. Des. 88, 1169–1173. https://doi.org/10.1016/j.cherd.2010.01.011

Mio, H., Kano, J., Saito, F., 2004. Scale-up method of planetary ball mill. Chem. Eng. Sci. 59, 5909–5916. https://doi.org/10.1016/j.ces.2004.07.020

Mio, H., Kano, J., Saito, F., Kaneko, K., 2004. Optimum revolution and rotational directions and their speeds in planetary ball milling. Int. J. Miner. Process. 74, 585–592. https://doi.org/10.1016/j.minpro.2004.07.002

Mishra, R.K., Geissbuhler, D., Carmona, H.A., Wittel, F.K., Sawley, M.L., Weibel, M., Gallucci, E., Herrmann, H.J., Heinz, H., Flatt, R.J., 2015. En route to multi-model scheme for clinker comminution with chemical grinding aids. Adv. Appl. Ceram. 114, 393–401. https://doi.org/10.1179/1743676115Y.0000000023

Mori, H., Mio, H., Kano, J., Saito, F., 2004. Ball mill simulation in wet grinding using a tumbling mill and its correlation to grinding rate. Powder Technol. 143–144, 230–239. https://doi.org/10.1016/j.powtec.2004.04.029

Mucsi, G., 2019. A review on mechanical activation and mechanical alloying in stirred media mill. Chem. Eng. Res. Des. 148, 460–474. https://doi.org/10.1016/j.cherd.2019.06.029

Panjipour, R., Barani, K., 2018. The effect of ball size distribution on power draw, charge motion and breakage mechanism of tumbling ball mill by discrete element method (DEM) simulation. Physicochem. Probl. Miner. Process. 54, 258–269. http://dx.doi.org/10.5277/ppmp1811

Patil, A.G., Anandhan, S., 2015. Influence of planetary ball milling parameters on the mechano-chemical activation of fly ash. Powder Technol. 281, 151–158. http://dx.doi.org/10.1016/j.powtec.2015.04.078

Rodriguez, V.A., Carvalho, R.M., Tavares, L.M., 2018. Insights into advanced ball mill modelling through discrete element simulations. Miner. Eng. 127, 48–60. https://doi.org/10.1016/j.mineng.2018.07.018

Rosenkranz, S., Breitung-Faes, S., Kwade, A., 2011. Experimental investigations and

modelling of the ball motion in planetary ball mills. Powder Technol. 15, 224–230. https://doi.org/10.1016/j.powtec.2011.05.021

Scott, L., Borissova, A., Burns, A., Ghadiri, M., 2021. Influence of holdup on gas and particle flow patterns in a spiral jet mill. Powder Technol. 377, 233–243. https://doi.org/10.1016/j.powtec.2020.08.099

Shashanka, R., Chaira, D., 2015. Optimization of milling parameters for the synthesis of nano-structured duplex and ferritic stainless steel powders by high energy planetary milling. Powder Technol. 278, 35–45. http://dx.doi.org/10.1016/j.powtec.2015.03.007

Suryanarayana, C., 2001. Mechanical alloying and milling. Prog. Mater. Sci. 46, 1–184. https://doi.org/10.1016/S0079-6425(99)00010-9

Tsuji, Y., Tanaka, T., Ishida, T., 1992. Lagrangian numerical simulation of plug flow of cohesionless particles in a horizontal pipe. Powder Technol. 71, 239–250. https://doi.org/10.1016/0032-5910(92)88030-L

Tuzcu, E.T., Rajamani, R.K., 2011. Modeling breakage rates in mills with impact energy spectra and ultra fast load cell data. Miner. Eng. 24, 252–260. https://doi.org/10.1016/j.mineng.2010.08.017

Vijay, B., Rehan, A., Jiri, M., 2013. Optimisation of ball milling parameters for refinement of waste jute fibres to nano/micro scale in dry conditions. J. Text. Eng. 59, 87–92. https://doi.org/10.4188/jte.59.87

Wang, M.H., Yang, R.Y., Yu, A.B., 2012. DEM investigation of energy distribution and particle breakage in tumbling ball mills. Powder Technol. 223, 83–91. https://doi.org/10.1016/j.powtec.2011.07.024

Nomenclature

C_1	Coefficient of Eq. (3) [W/kg]
C_2 and C_3	Coefficients of Eq. (3) [–]
D_b	Ball diameter [m]
D_p	Particle diameter [m]
E	Dissipated energy of particles at a single particle collision [J]
E_{min}	Size-independent material property referred to as the threshold energy of breakage [J·m/kg]
E_s	Specific dissipated power of particles exceeding a threshold E_{th} [W/kg]
E_{th}	Threshold energy of particle breakage at a single particle collision [J]
F_n	Normal contact force [N]
F_t	Tangential contact force [N]
m_b	Mass of single ball [kg]
m_p	Mass of single particle [kg]
N_b	Number of balls [–]
N_p	Number of particles [–]
t	Milling time [s]
t_c	Contact period [s]
δ_n	Normal overlap [m]
δ_t	Tangential overlap [m]

Figure and table captions

Table 1 Parameters used in simulations.

Table 2 Sizes and numbers of particles and balls used in simulations.

Table 3 Example of variation in milling conditions with decreasing particle size to maintain energy.

Fig. 1. Typical change in specific dissipated power of particles with milling time.

Fig. 2. Snapshots of behaviors of particles and balls mimicking various stages of particle breakage at different values of BPR (D_b = 10 mm).

Fig. 3. Effect of D_p on dissipated energy distribution of all collisions at different values of BPR (D_b = 10 mm).

Fig. 4. Effect of D_p on E_s for particle-to-ball, particle-to-wall, and particle-to-particle collisions at BPR = 30 and 5 (D_b = 10 mm).

Fig. 5. Variations in E_s for all collisions with respect to D_p and BPR (D_b = 10 mm).

Fig. 6. Changes in behaviors of particles and balls with ball size at different values of BPR (D_p = 2.0 mm).

Fig. 7. Effect of D_b on dissipated energy distribution of all collisions at different values of BPR (D_p = 2.0 mm).

Fig. 8. Effect of D_b on E_s for particle-to-ball, particle-to-wall, and particle-to-particle collisions at BPR = 30 and 5 (D_p = 2.0 mm).

Fig. 9. Variations in E_s for all collisions with respect to D_b and BPR (D_p = 2.0 mm).

Fig. 10. Application of Eq. (4) for estimating E_s.

Fig. 11. Effect of changing D_b and N_b on variation in E_s with particle breakage stage.